J.M. Dailey and T.L. Koch, “Impact of Carrier Heating on SOA Transmission Dynamics for Wavelength Conversion”, *Photonics Technology Letters*, **19** (14), pp 1078-1080, 2007.

http://ieeexplore.ieee.org/search/srchabstract.jsp?tp=&arnumber=4252134&queryText%3Dj.m.+dailey%26openedRefinements%3D*%26filter%3DAND%28NOT%284283010803%29%29%26searchField%3DSearch+All

Impact of Carrier Heating on SOA Transmission Dynamics for Wavelength Conversion

James M. Dailey, *Student Member, IEEE* and Thomas L. Koch, *Fellow, IEEE*

***Abstract*— Complex-valued time-resolved transmission characteristics of a semiconductor optical amplifier (SOA) are measured using a spectrogram technique. A relatively simple traveling-wave density matrix model is implemented that accurately captures the evolution of complex index due to stimulated emission and carrier heating. The model shows good agreement with experimental spectrogram data.**

***Index Terms*—Semiconductor Optical Amplifiers, Semiconductor Device Modeling, Optical Frequency Conversion, Hot Carriers**

I. Introduction

All-optical wavelength converters based on cross-phase modulation in semiconductor optical amplifiers (SOAs) are promising candidates for future high-speed all-optical data routing applications. Integrated interferometer designs have been extensively studied, and more recently, arrangements using SOAs with a trailing-filter [1]-[2] have also shown promise. As bit rates escalate to 40 Gb/s and beyond, a number of interesting signatures emerge including distinctly different amplitude and phase recovery times, which suggests the inapplicability of often-used α-factor models. Sophisticated pump-probe experimental studies and comprehensive theoretical analyses have elucidated the roots and rich nature of ultrafast SOA dynamics, especially on the subpicosecond timescale; see e.g. [3]-[5]. However, to assist in the design of more complex network applications of SOA wavelength converters, streamlined experimental and modeling validation techniques may be helpful in evaluating eye-margin degradation against system parameters, e.g. variations in SOA drive, pulse signal wavelength, power, duty cycle, pre- and post-filtering, cascaded operation, etc.

In this letter we report on experimental work using an inexpensive spectrogram technique that captures the most salient SOA amplitude and phase dynamical saturation behavior critical to 40 Gb/s operation [6]. We also model the gain and refractive index through rate equations governing the evolution of the Fermi-Dirac carrier distributions. This model illustrates that the innate first-principles temperature dependence of gain and refractive index, in conjunction with the key carrier heating sources of stimulated emission and free-carrier absorption, appears to capture the experimentally observed features without introducing any alpha factors or other linearization approximations. This paired modeling tool and spectrogram technique allow simple variations of experimental conditions, and should provide a useful approach for system-level design and validation of wavelength converters in next-generation networks.

Section II describes the experimental setup, section III provides details on the model, a discussion of the results are in section IV, and conclusions are summarized in section V.

II. Experiment

We implemented a linear spectrographic technique [7] to measure complex transmission characteristics of a bulk SOA device, approximately 1 mm in length, biased at 200 mA. The gain peak is at 1543 nm. As depicted in Fig 1a, a mode-locked laser provides 2 ps pump pulses at 1550 nm at 10 GHz. Probe pulses at 1560 nm with a 20 ps width are generated by an electro-absorption modulator and co-injected into the SOA device. Pump pulse energy was 66 fJ while the probe energy was 23 dB less. The RF phase shifter incrementally steps through the 100 ps period to

Manuscript received Nov. 15, 2006 and revised Apr. 6, 2007. This work was supported by the DARPA DOD-N IRIS project.

J. M. Dailey and T. L. Koch are with the Center for Optical Technologies, Lehigh University, Bethlehem, PA 18015 USA (610-758-5164, email: jmd3@lehigh.edu).

control the pump-probe temporal delay. The altered probe spectrum is captured on an optical spectrum analyzer (OSA) at each temporal step. Each of these spectra comprises a column in the spectrogram data matrix. The numerical processing of this spectrogram yields the SOA's complex transfer function [7] along with the complete amplitude and phase envelope for the probe, apart from trivial ambiguities which are of no consequence [8]-[9].

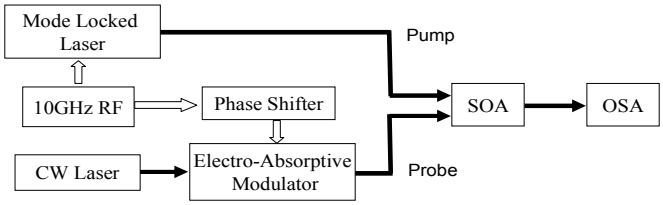

Fig 1a. Setup for obtaining spectrograms.

Processing the spectrogram involves a double-blind deconvolution that has been used in Frequency Resolved Optical Gating (FROG). The spectrogram is injected into a Principal Components Generalized Projections Algorithm (PCGPA) [8], which yields the time resolved complex SOA transmission function. The deconvolution begins with an initial "known" probe pulse function to aid in convergence [9]. A portion of a typical spectrogram is shown in Fig 1b, illustrating the large amount of chirp on the probe near t = -12 ps where the pump and probe pulses have close temporal alignment.

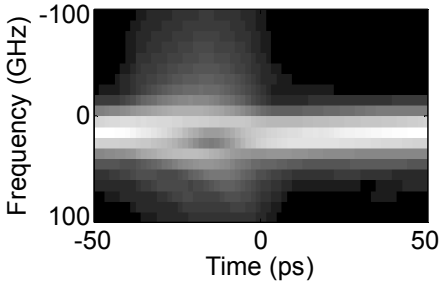

Fig 1b. Portion of a typical spectrogram measured from SOA output spectra.

The normalized PCGPA output is shown in Fig 2. The phase, whose derivative yields SOA chirp, is seen to recover significantly more slowly than the intensity, which is a measure of SOA gain.

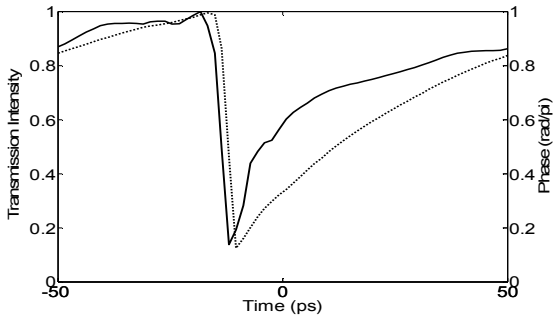

Fig 2. Normalized SOA transmission intensity (solid) and phase (dot) obtained from spectrogram measurement.

These data are very similar to results recently published by Giller *et al.* [10] using a TOAD pump/probe configuration.

III. MODEL

The device behavior is modeled with traveling-wave rate equations for photon density, optical phase, carrier concentration, and carrier temperature. The computation dynamically evaluates the spatial and temporal variation of

the real and imaginary index of refraction derived from a Maxwell-Bloch density matrix analysis [11], obviating the need for any linearization or alpha factor approximations. Two-photon absorption, using known parameters, is incapable of producing loss transients of the magnitude observed for our pump intensity [4]. Similarly, the stimulated emission rate, relative to intraband scattering rates [4], is insufficient to produce spectral hole burning at the observed level. For these reasons we use equilibrium Fermi-Dirac distributions and focus on the evolution of the carrier temperature. This approximation may not be valid for higher power levels and shorter timescales.

The complex refractive index calculated from the density matrix model is given by (1) below. The imaginary part of (1) corresponds to the gain, and the real part contains the contribution to the refractive index of the resonant band-to-band transitions:

$$\tilde{n}(\omega) = \frac{\mu_{cv}^2}{4\pi\varepsilon_0 n}\left(\frac{2m_r}{\hbar^2}\right)^{3/2} \cdot \int_0^\infty (f_e + f_h - 1)\sqrt{\hbar\Omega}\,\frac{\left[i\cdot\frac{1}{\pi}T_2 + \frac{1}{\pi}\left(\omega - \frac{E_g}{\hbar} - \Omega\right)T_2^2\right]}{1 + \left(\omega - \frac{E_g}{\hbar} - \Omega\right)^2 T_2^2}\,d\Omega \tag{1}$$

The dephasing time is taken to be $T_2 \sim 150$ fs, while ω, μ_{cv}, m_r, n, and E_g represent the optical angular frequency, dipole matrix element, reduced mass, background (non-resonant) refractive index, and bandgap energy, respectively. The f_e and f_h denote the electron and hole Fermi-Dirac distribution functions which depend on temperature and carrier density through their respective Fermi energies.

The rate equations used are:

$$\left(\frac{\partial}{\partial t} \pm v_g \frac{\partial}{\partial z}\right) S_\omega^{\pm} = v_g \Gamma S_\omega^{\pm}\left(g_\omega - \alpha_{FC} N\right) + R_{sp,\omega} \tag{2}$$

$$\left(\frac{\partial}{\partial t} + v_g \frac{\partial}{\partial z}\right)\varphi_\omega = v_g \Gamma \frac{\omega}{c}\left(\delta n_{b-b,\omega} + \delta n_{plasma,\,\omega}\right) \tag{3}$$

$$\frac{dN}{dt} = \frac{I}{qV} - v_g \sum_\omega g_\omega \cdot \left[S_\omega^{+} + S_\omega^{-}\right] - bN^2 - cN^3 \tag{4}$$

$$\frac{dT}{dt} = \frac{1}{\frac{\partial U}{\partial T}} \cdot \left(\frac{dU}{dt} - \frac{\partial U}{\partial N}\frac{dN}{dt}\right) - \frac{T - T_0}{\tau} \tag{5}$$

Equation (2) contains the forward (S_ω^{+}) and reverse (S_ω^{-}) propagating photon densities at the frequencies of interest, including pump and probe signals as well as amplified spontaneous emission. The group velocity, confinement factor, gain, and spontaneous emission rate are given by v_g, Γ, g_ω, and R_{sp}, respectively. The rate of free carrier and inter-valence-band (IVB) absorption is controlled by α_{FC}.

Equation (3) describes the phase evolution along the amplifier with contributions from both resonant interband transitions ($\delta n_{b\text{-}b,\omega}$) and the free-carrier plasma ($\delta n_{plasma,\omega}$), where the Drude model is used for the latter refractive index change. The carrier density (N) equation is shown in (4) where b and c are the usual bimolecular and Auger recombination coefficients, respectively.

The temperature dynamics are described by (5), where electron and hole plasmas are assumed equal in both density N and temperature T, while U is the total plasma energy density. The term dU/dt is easily evaluated using simple expressions for the rate of energy change from stimulated emission as well as free carrier and IVB absorption, while the other derivatives on the r.h.s. are easily evaluated from the Fermi-Dirac distribution functions. The last term on the r.h.s. of (5) represents temperature relaxation with a phenomenological time constant τ rather than implementing a first-principles dynamical electron-phonon carrier cooling model.

The device's intensity transmission Θ is easily evaluated from the temperature and carrier-dependent material gain:

$$\Theta(t) = e^{\Gamma\Delta z\sum_{n=1}^{M} g_n\left(t - [M-n]\frac{\Delta z}{v_g}\right)} \tag{6}$$

where the device has been divided into M sections each of length Δz, and $g_n(t)$ is the time dependent net material gain (i.e. including losses) in the n^{th} section. The SOA transmission phase is given by the solution of (3). A finite difference technique is used to solve (1)-(5) numerically. Typical computation times are below 10 minutes, allowing the model to be useful for design iterations. Material parameters are chosen based on conventional values, see e.g. [12].

IV. MODEL RESULTS

Figure 3a shows the calculated SOA transmission based on estimated device parameters and is seen to have good agreement with the major features of the measurement. While the intensity displays a pronounced fast component followed by a slower recovery, the fast component of the phase recovery is almost absent.

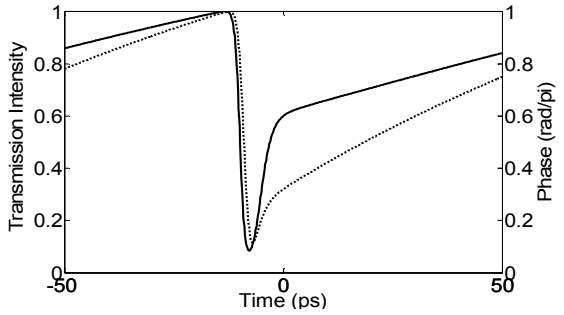

Fig. 3a. Model output showing normalized intensity (solid) and phase (dot) transmission of SOA.

This behavior is understood by noting that the pump pulse heats the carrier plasma due to stimulated emission as well as free carrier and IVB absorption. Fig. 3b illustrates clearly, on an expanded timescale, the saturation and subsequent rapid partial gain recovery due to the cooling of the plasma. The slower component of the gain recovery then results from the overall replenishment of depleted carriers by injection current.

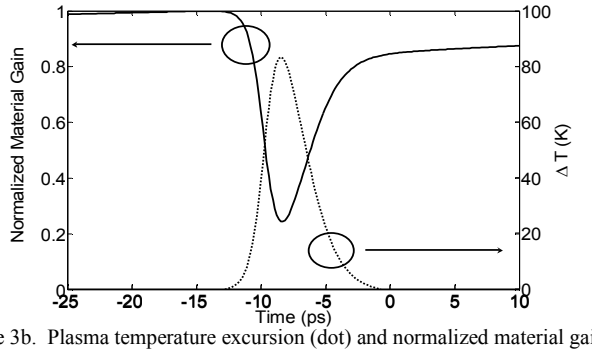

Figure 3b. Plasma temperature excursion (dot) and normalized material gain coefficient (solid) near the SOA exit facet.

The phase transient has a much less pronounced fast component, which results from two distinct effects. Firstly, the resonant component $\delta n_{b\text{-}b,\omega}$ responds less to temperature transients than does the gain, which can be understood by inspection of (1). The temperature dependence of $\tilde{n}$ enters through the Fermi functions which multiply imaginary and real components of the Lorentzian broadening function. The real component is inherently less localized in frequency (or energy) than the imaginary (gain) component, and as a consequence the integrated real index is less sensitive to the changes in the Fermi distributions with temperature. Secondly, the free-carrier plasma contribution $\delta n_{plasma,\omega}$ is of comparable magnitude to $\delta n_{b\text{-}b,\omega}$ and has no pronounced temperature dependence. As a result, the plasma temperature excursions have less effect on transmission phase, which instead primarily tracks carrier density recovery with injected current.

In Figure 3a we have used a plasma temperature relaxation time of $\tau \sim 1$ ps in (5), which is seen to provide good agreement with our experimental data. This value is consistent with other reports of plasma temperature relaxation

in regimes of high excitation and phonon populations [13].

V. CONCLUSIONS

The inclusion of a temperature rate equation with key heat sources and a first-principles complex index evaluation produces model results in good agreement with high-speed, high-saturation SOA spectrogram measurements. These experimental and modeling tools should prove useful for system design and validation in 40 Gb/s systems incorporating SOA-based wavelength conversion.

VI. REFERENCES

[1] H. Chayet, *et al.*, "Regenerative all-optical wavelength converter based on semiconductor optical amplifier and sharp frequency response filter," in *OFC*, Los Angeles, CA, 2004, Paper ThS2.

[2] J. Leuthold, "Semiconductor optical amplifier-based devices for all-optical high-speed wavelength conversion," in *Optical Amplifiers and Their Applications Conference*, Stresa, Italy, 2001, Paper OWA1.

[3] K. L. Hall, E. R. Thoen, and E. P. Ippen, "Nonlinearities in active media," in *Semiconductors and Semimetals,* vol. 59, E. Garmire and A. Kost, Eds., Academic Press, 1999, pp. 83-160.

[4] J. Mark and J. Mork, "Subpicosecond gain dynamics in InGaAsP optical amplifiers: experiment and theory," *Appl. Phys. Lett.,* vol. 61, no. 19, pp. 2281-2283, Nov. 1992.

[5] A. Mecozzi and J. Mork, "Saturation effects in nondegenerate four-wave mixing between short optical pulses in semiconductor laser amplifiers," *IEEE J. Sel. Top. Quantum Electron.,* vol. 3, no. 5, pp. 1190-1207, 1997.

[6] J. M. Dailey and T. L. Koch, "Impact of carrier heating on SOA dynamics for wavelength conversion," in *IEEE LEOS*, Montreal, QC, Canada, 2006, Paper MP4.

[7] I. Kang and C. Dorrer, "Measurements of gain and phase dynamics of a semiconductor optical amplifier using spectrograms," in *OFC*, Los Angeles, CA, 2004, Paper MF43.

[8] D. J. Kane, "Recent progress toward real-time measurement of ultrashort laser pulses," *IEEE J. Quantum Electron.,* vol. 35, no. 4, pp. 421-431, 1999.

[9] C. Dorrer and I. Kang, "Real-time implementation of linear spectrograms for the characterization of high bit-rate optical pulse trains," *IEEE Photon. Technol. Lett.,* vol. 16, no. 3, pp. 858-860, 2004.

[10] R. Giller, R. J. Manning, and D. Cotter, "Gain and phase recovery of optically excited semiconductor optical amplifiers," *IEEE Photon. Technol. Lett.,* vol. 18, no. 9, pp. 1061-1063, 2006.

[11] A. Yariv, *Quantum Electronics,* 3rd ed., John Wiley & Sons, 1989, ch. 8.

[12] L. A. Coldren and S. W. Corzine, *Diode lasers and photonic integrated circuits,* John Wiley & Sons, 1995.

[13] J. Shah, *Ultrafast spectroscopy of semiconductors and semiconductor nanostructures,* 2nd enl. ed., Springer-Verlag, 1999.